Coiled-coil networking shapes cell molecular machinery

Yongqiang Wang[a,*], Xinlei Zhang[a,b,*], Hong Zhang[a,*], Yi Lu[a,b], Haolong Huang[a], Xiaoxi Dong[a,b], Jinan Chen[a,b], Jiuhong Dong[a], Xiao Yang[a,b], Haiying Hang[a], and Taijiao Jiang[a]
[a]National Laboratory of Biomacromolecules, Institute of Biophysics, Chinese Academy of Sciences, Beijing 100101, China; [b]Graduate School, Chinese Academy of Sciences, Beijing 100080, China

ABSTRACT **The highly abundant α-helical coiled-coil motif not only mediates crucial protein–protein interactions in the cell but is also an attractive scaffold in synthetic biology and material science and a potential target for disease intervention. Therefore a systematic understanding of the coiled-coil interactions (CCIs) at the organismal level would help unravel the full spectrum of the biological function of this interaction motif and facilitate its application in therapeutics. We report the first identified genome-wide CCI network in *Saccharomyces cerevisiae*, which consists of 3495 pair-wise interactions among 598 predicted coiled-coil regions. Computational analysis revealed that the CCI network is specifically and functionally organized and extensively involved in the organization of cell machinery. We further show that CCIs play a critical role in the assembly of the kinetochore, and disruption of the CCI network leads to defects in kinetochore assembly and cell division. The CCI network identified in this study is a valuable resource for systematic characterization of coiled coils in the shaping and regulation of a host of cellular machineries and provides a basis for the utilization of coiled coils as domain-based probes for network perturbation and pharmacological applications.**

Monitoring Editor
Kerry S. Bloom
University of North Carolina

Received: May 29, 2012
Revised: Jul 31, 2012
Accepted: Aug 2, 2012

INTRODUCTION

The coiled-coil motif, which consists of two or more α-helices twisted around one another, is one of the most frequently encountered interacting motifs in nature (Crick, 1953; Rose and Meier, 2004; Lupas and Gruber, 2005). Coiled coils are present in ~10% of the eukaryotic proteome (Liu and Rost, 2001). Many studies have shown that coiled-coil interactions (CCIs) underlie a variety of cellular functions, including dynamic assembly of protein complexes (Rose and Meier, 2004), transcription (O'Shea *et al.*, 1991, 1992), intracellular trafficking (Gillingham and Munro, 2003), and viral infection (Carr and Kim, 1993; Eschli *et al.*, 2006). Owing to its crucial roles in many physiological and pathological processes, the coiled-coil motif has emerged as a potential target for the intervention of a large number of diseases in which coiled coils play a role (Strauss and Keller, 2008). A notable example is the design of coiled-coil inhibitors to interfere with viral entry during HIV infection (Wild *et al.*, 1992; Kilby *et al.*, 1998).

Coiled coils have recently attracted much attention in the fields of material science (Lomander *et al.*, 2005) and synthetic biology (Bromley *et al.*, 2008; Robson Marsden and Kros, 2010). Owing to the simplicity of their structure (Parry, 1982; Lupas *et al.*, 1991), specificity of interaction (Mason *et al.*, 2006; Grigoryan *et al.*, 2009), reversible association, and prevalence (Rose and Meier, 2004), coiled coils have became a popular template for the design of molecular circuits (Wu *et al.*, 2009), biosensors (Shekhawat *et al.*, 2009), and molecular electronic devices (Shlizerman *et al.*, 2010), and the engineering of biomaterials for drug delivery (Boato *et al.*, 2007; McFarlane *et al.*, 2009).

Despite the biological significance and wide application of coiled coils, a comprehensive picture of how they are associated in the cell is lacking. In this study, we used the yeast two-hybrid assay (Y2H) approach to map the interactions of 893 coiled coils predicted for *Saccharomyces cerevisiae*, which allowed us to gauge the designing

This article was published online ahead of print in MBoC in Press (http://www.molbiolcell.org/cgi/doi/10.1091/mbc.E12-05-0396) on August 8, 2012.

*These authors contributed equally to this work.

Address correspondence to: Taijiao Jiang (taijiao@moon.ibp.ac.cn).

Abbreviations used: BiFC, bimolecular fragmentation complementation assay; CCI, coiled-coil interaction; CCP, coiled-coil protein; CCPI, coiled-coil protein interaction; EGFP, enhanced green fluorescent protein; GO, Gene Ontology; RFP, red fluorescent protein; SC medium, synthetic medium; SNARE, soluble *N*-ethylmaleimide sensitive; t-SNARE, target membrane SNARE; v-SNARE, vesicular SNARE; Y2H, yeast two-hybrid assay; YPDA, yeast peptone dextrose adenine.

principles and functions of the CCI network in budding yeast at the genome level. The physiological relevance of the CCI network was demonstrated by the crucial roles of coiled-coil–mediated interactions in shaping the structure and function of the kinetochore. The genome-wide mapping of the yeast CCI network not only offers systems-level insights into the organization of a number of yeast cellular machineries, but also provides a framework on which new strategies may be developed for modulation of protein complexes that are mediated by coiled coils. This would allow further insight into biological processes, such as the cell cycle, cell division, and intracellular trafficking, and could enable the treatment of human diseases in which the CCI network is altered.

RESULTS

Identification of the coiled-coil interactome in yeast

Using the sequence-based prediction program Paircoil2 (McDonnell *et al.*, 2006), we predicted 899 coiled coils in 637 proteins from the 6720 annotated yeast proteins (Supplemental Table S1). The predicted coiled-coil–containing proteins, or coiled-coil proteins (CCPs), constitute ~10% of the yeast proteome, which indicates their prevalence. On average, a predicted coiled coil is made up of 63 amino acids. A typical protein identified herein contains 1.8 coiled coils, which is ~11.6% of the length of the parent protein (Supplemental Figure S1). The yeast CCPs, which are involved in a wide variety of cellular functions (Table S2), are particularly enriched in processes such as gene transcription, the cell cycle, intracellular trafficking, and structural organization of the cell (p value < 0.05; Figure S2A).

Given the prevalence of coiled coils in nature and their roles in mediating protein interactions, we sought to gain a comprehensive picture of coiled-coil networking in the budding yeast. We cloned 893 of the 899 predicted coiled coils from the yeast genome and carried out a large-scale analysis of their interactions using the Y2H system (Figures 1A and S2B). This analysis identified 3495 pairs of interactions among 598 coiled-coil motifs in 453 proteins. (A list of positives from the Y2H screen is provided in Table S3.) Further, we carried out independent tests to assess the quality of our CCI network. We first checked how well our data matched with the 237 pairs of CCIs previously identified by Newman *et al.* (2000). Our work recapitulated 94 (or ~40%) of these interactions. While the overlap is significant (p value < 0.01), the discrepancy may be due to the different coiled-coil regions used in the two studies. To obtain a more rigorous assessment of the quality of our CCI network, we subjected a fraction of the Y2H data to a test using the orthogonal, bimolecular fragmentation complementation assay (BiFC; Hu *et al.*, 2002). We first validated the positive CCIs identified within the kinetochore, a molecular machine controlling segregation of sister chromosomes during cell division (Kline-Smith *et al.*, 2005; Westermann *et al.*, 2007). Of the 54 CCIs identified among kinetochore proteins, 36 (or 66.7%) were verified by BiFC. We then randomly selected 23 cell cycle–related coiled coils and tested the 32 interactions between them using BiFC; this confirmed 15 (46.9%) as positives. We also tested the interactions identified by Y2H between the 23 cell-cycle coiled coils and 27 coiled coils involved in vesicular trafficking that had previously been analyzed (Zhang *et al.*, 2009). Of 55 Y2H-identified interactions, 24 (43.6%) were verified by BiFC (Table S4). Given the stringent requirements of the BiFC method (Kerppola, 2008), this suggests that the CCI network identified by Y2H is of high quality. The reliable mapping of the yeast coiled-coil interactome provides an unprecedented opportunity to gain a systematic understanding of the functions of coiled coils.

The yeast CCI network is specific and functionally organized

We processed the CCI data as a network in which nodes are coiled-coil motifs and edges represent interactions between them (Figure 1A). To characterize the organizational principles of the CCI network, we compared this motif-level interaction map with the CCP interaction (CCPI) network, the latter of which was constructed based on reported physical interactions among yeast proteins (Figure 1A). We found that the two networks are comparable in terms of general network properties, such as average connectivity, average clustering coefficient, and network connectivity (see the Supplemental Materials and summaries of analysis in Figure S3 and Table S5), suggesting that the two networks have similar characteristics. Figure 1B shows that the CCI network, similar to the CCPI network, exhibits a power-law distribution of its node degree (i.e., the number of interactions mediated by a coiled coil). In particular, we found a small number of coiled coils have a high degree of connectivity (i.e., ≥10), but most (>65.7%) exhibit a low degree of connectivity characterized by fewer than 10 interacting partners (Figure S4), indicating that the interactions between most of the stand-alone coiled coils are highly specific (Barabasi and Oltvai, 2004).

To learn whether the CCIs are organized into functional modules, we calculated modularity of the CCI network, a measure of how similar the function of a protein is to those of its neighbors (Ravasz *et al.*, 2002; Komurov and White, 2007; see the Supplemental Materials). We found that the CCI network has a significantly higher network modularity (0.679; Figure 1C) than that of randomized networks (0.406 ± 0.022, p value < 0.0001), demonstrating that the coiled-coil motif, albeit a general interaction motif, tends to mediate interactions between proteins that are functionally related. However, the functional relatedness of the CCI network is much lower than that of the CCPI network (1.329). Interestingly, when the reported CCPI network obtained from three large-scale experiments (Uetz *et al.*, 2000; Ito *et al.*, 2001; Tarassov *et al.*, 2008) is considered, its network modularity is only 0.6056, which is close to, but a bit lower than, that of CCI network. We argue that the very high functional relatedness of the reported CCPIs may result from the small-scale experiments, which were mainly focused on the functionally related proteins.

Identifying high-probability, coiled-coil–mediated protein interactions from the Y2H CCI data

Because coiled coils constitute only a small portion of most CCPs, the interactions between the stand-alone coiled coils may not account for their parent protein interactions. Therefore we developed a probabilistic model to identify high-probability, coiled-coil–mediated protein interactions. This process can also serve to filter out the false-positive interactions from the Y2H data. To infer coiled-coil–mediated protein interactions from the original CCI data, we used a scoring system to estimate the likelihood of a pair of coiled coils mediating a corresponding protein–protein interaction (Figure 2A; see also *Materials and Methods*). We started by separating the 3210 unique, CCI-derived protein pairs (homodimeric CCP pairs were not included) into two groups. The first group comprised 196 pairs of experimentally verified interacting proteins, or high-confidence coiled-coil–mediated protein interactions, which were used as "positives," because these interactions occur at both the coiled-coil motif and the protein level. The remaining 3014 CCI-derived protein interactions were placed in the unlabeled CCI data group. We then developed a three-step strategy to identify coiled-coil–mediated protein interactions from the unlabeled CCI data. This strategy was based on the integration of several features of the coiled-coil motif and the corresponding protein that were shown to effectively

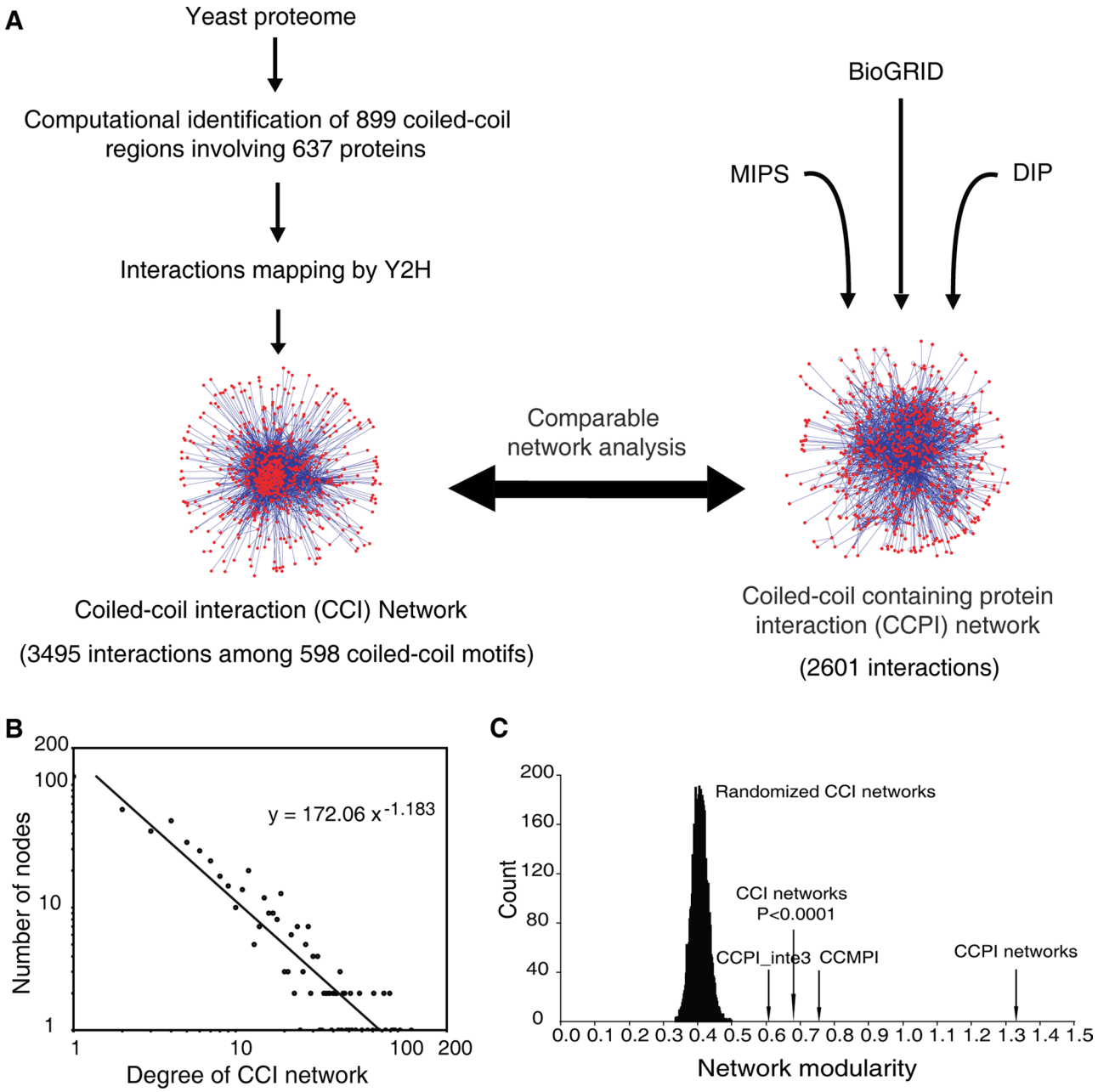

FIGURE 1: Genome-wide analysis of coiled coils and their interactions in *S. cerevisiae*. (A) A flowchart for genome-wide identification of the CCI map in yeast. (B) Degree distribution of the CCI network identified from a large-scale Y2H screening. The CCI network was a scale-free network, with a power-law degree distribution of its nodes following $P(k) \sim k^{-\gamma}$, $\gamma = 1.183$. (C) The modularity of the CCI network compared with that of randomized CCI networks, reported CCP interactions obtained from both large-scale and small-scale experiments (CCPI network), and reported CCP interactions obtained from three high-throughput interactome mapping (CCPI_inte3 network; Uetz *et al.*, 2000; Ito *et al.*, 2001; Tarassov *et al.*, 2008) or computational inferred coiled-coil–mediated protein interaction mapping (CCMPI network). CCPI_inte3, large-scale experiment protein interaction map; CCMPI, inferred coiled-coil–mediated protein interaction map; CCPI networks, large-scale experiment plus small-scale experiment protein interaction map.

discriminate between the positive and the unlabeled CCI data (Figure 2A). Briefly, we first identified the general factors, including the expression property and essentiality of a CCP, and the size and connectivity of its coiled coils, all of which could contribute to the identification of coiled-coil–mediated protein interactions from a given set of CCIs (Table S6). We next measured the ability of each factor to discriminate the positive data from the unlabeled data by calculating a likelihood ratio [$L = P$(data set|pos) ÷ P(data set|unlabel)], a ratio of the probability of identifying a coiled-coil–mediated protein interaction from the positive data set to the probability of identifying a coiled-coil–mediated protein interaction from the unlabeled data set (Table S6). Finally, we assigned a confidence score for each CCI pair in the unlabeled data set that reflects the cumulative contributions of all factors as a product of the likelihood ratios. Figure 2B shows that the retention of the unlabeled data decreased much more rapidly than that of the positive data with increasing confidence

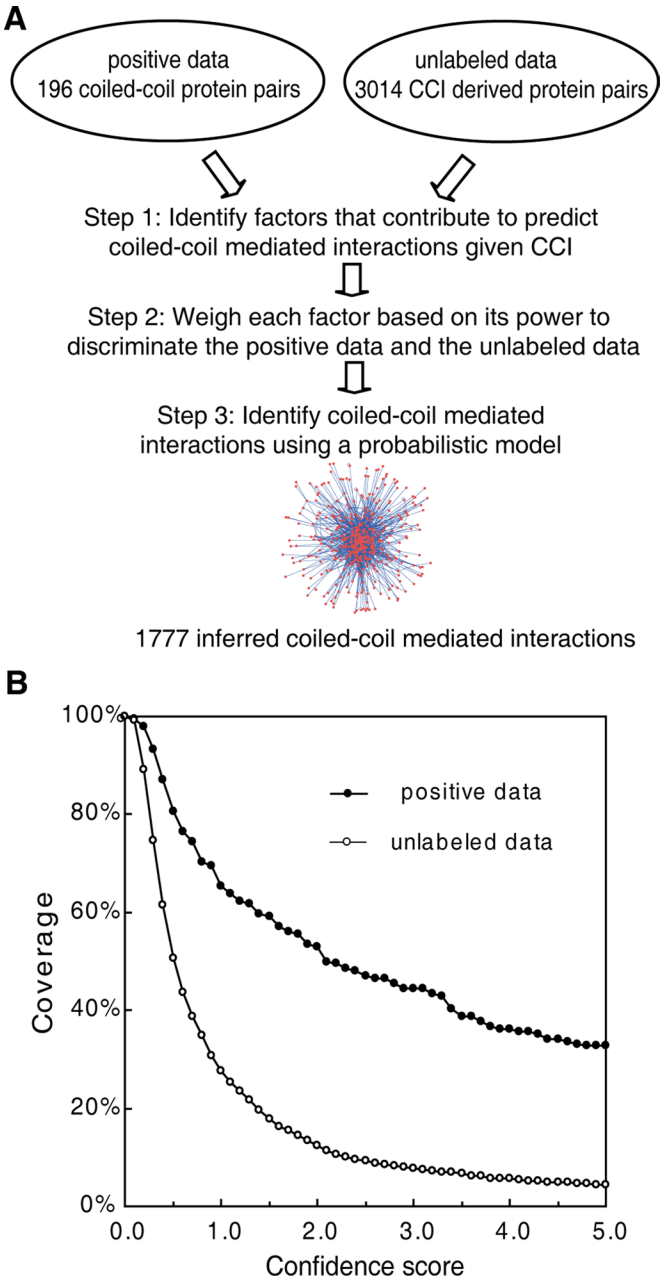

FIGURE 2: Properties of the CCI network. (A) A flowchart illustrating the computational strategies used to infer coiled-coil–mediated protein interactions. (B) Cumulative distribution of the coverage of positive and unlabeled data against the confidence score, the product of the likelihood ratios of individual factors. The accuracy of predicting coiled-coil–mediated protein interactions can be assessed by the coverage ratio between the positive data and the unlabeled data; the higher the coverage ratio, the more accurate the inference of the coiled-coil–mediated protein interactions. However, the accuracy and sensitivity of predictions are compromised; increases in the coverage ratio (i.e., the accuracy) come with a decrease in the coverage of positives (i.e., the sensitivity). We deemed protein pairs with a confidence score of ≥ 0.5 as the predicted coiled-coil–mediated protein interactions.

score, indicating the high accuracy of the prediction. The confidence scores of 3014 coiled-coil–derived protein pairs are given in Table S7. To gain a comprehensive picture of the functional roles of the CCI network, we deemed the 1529 protein pairs with a confidence score ≥0.5 as the predicted coiled-coil–mediated protein interactions (Figure 2B). At this cutoff, a high retention rate of the positive data (~80%) and a moderate retention rate of unlabeled data (~40%) were achieved. A total of 1777 protein interactions were identified as coiled-coil–mediated protein interactions when the positive and predicted interactions were combined (Table S7). The inferred coiled-coil–mediated protein interaction network has a higher network modularity (0.753) than the CCI network (Figure 1C), indicating its greater functional relatedness

Functional characterization of the coiled-coil–mediated protein interaction network

Figure 3 shows the participation of coiled-coil–mediated protein interactions in biological processes according to gene ontology (GO) annotations (Ashburner *et al.*, 2000). Our analysis shows that the identified coiled-coil–mediated protein interactions are involved in a variety of biological processes, including vesicle-mediated transport, cellular membrane organization, cytokinesis, and chromosome segregation. Some of these pathways, such as chromosome segregation and vesicle-mediated transport, are not only conserved between yeast and humans but are also closely related to human diseases, such as cancer and Parkinson's disease. Further analysis of the molecular functions of the CCI-derived protein pairs shows that CCIs occur mainly between proteins involved in binding and motor activity, rather than between proteins involved in catalysis and metabolism (Figure S5A). This is in agreement with previous reports that coiled coils mediate multifaceted protein–protein oligomerizations (Lupas and Gruber, 2005).

Identification of coiled-coil molecular machines in yeast

The identification of putative coiled-coil–mediated protein interactions allowed us to examine the role of coiled coils in mediating the organization of the yeast cellular machinery. Notably, we found that the enrichment of the identified coiled-coil–mediated protein interactions in same cellular component is significant compared with the enrichment anticipated for its randomized networks ($p < 0.05$). As shown in Figure S5B, coiled-coil–mediated interactions are enriched in such cellular structures or localizations as the cytoskeleton, bud, cell cortex, and sites of polarized growth. We implemented a more precise colocalization analysis of CCIs using the complex information in the GO database and found that coiled-coil associations are significantly enriched within protein complexes ($p < 0.0001$), indicating a general role of coiled coils in the assembly of protein machinery in the cell.

Figure 4A highlights the CCIs within or between known protein complexes involved in gene transcription, protein modification and degradation, protein translation, membrane fusion, or cell cycle control. To characterize the physiological functions of coiled coils, we focused on protein complexes that are significantly enriched for both CCPs and coiled-coil–mediated interactions, which we denote as *coiled-coil molecular machines* (Table S8). We found that protein complexes involved in the organization or regulation of the cytoskeleton, kinetochore, or intracellular transport not only possess a significantly higher proportion of CCPs (51.9%, 42.9%, and 30.1% respectively), but are also significantly enriched for CCIs (p value <0.05; Figure 4B). The identification of these coiled-coil molecular machines underscores the critical roles of coiled coils in mediating the assembly and function of these protein complexes, an assertion that is supported by previous observations. For example, specific coiled-coil associations within the membrane fusion machinery, the soluble *N*-ethylmaleimide–sensitive

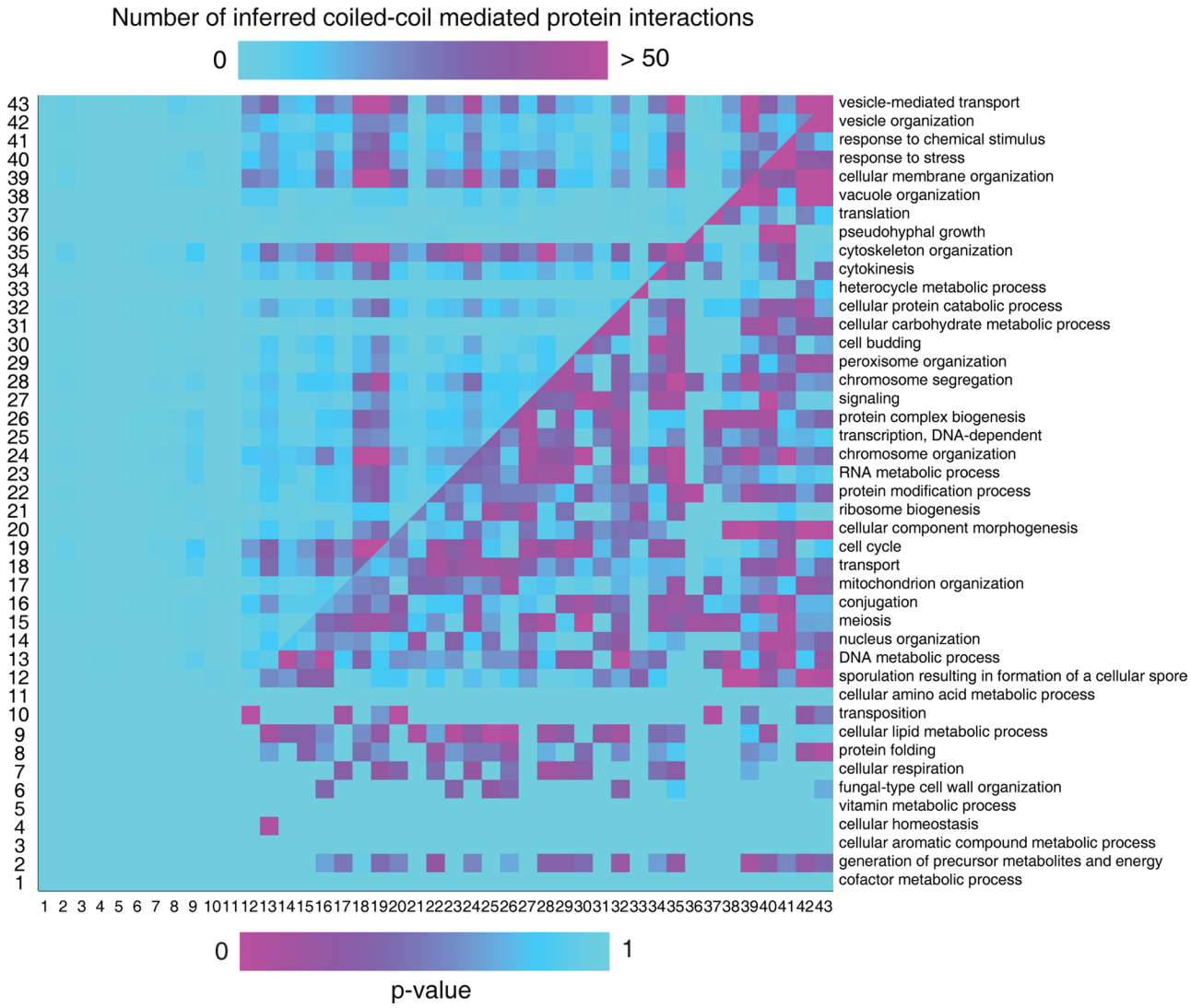

FIGURE 3: Distribution of CCIs across the biological process of GO slim annotation. Number of CCIs within or across the biological process of GO slim annotation (upper part of the matrix). Functional entries of each coiled coil were assigned from its parental protein's annotation directly. The extent of enrichment was measured by *p* value. The 43 annotations were sorted according to their *p* value and arranged in the chart from top to bottom.

(SNARE) complexes, are generally thought to drive membrane fusion in cellular trafficking (Ungar and Hughson, 2003; Jahn and Scheller, 2006). In this work, a mass of CCIs have been identified between vesicular SNAREs (v-SNAREs) and target membrane SNAREs (t-SNAREs), while far fewer interactions were observed within v-SNAREs or t-SNAREs (Figure S6A). This indicates that coiled-coil motifs contribute to binding specificity within SNARE heterotetramers. As for the cytoskeleton, previous studies have suggested the involvement of CCIs in mediating the association of motor proteins (Schliwa and Woehlke, 2003) and organizing filamentary structures, such as in paired septin filaments (Bertin *et al.*, 2008). We have identified an array of CCIs within the cytoskeleton (Figure S6B). In the case of the septin components, in addition to the capture of the previously reported coiled-coil–mediated interaction (Cdc3p-Cdc12p), we have discovered two novel coiled-coil–mediated interactions, Cdc3p-Cdc11p and Cdc12p-Spr3p. Our data suggest a critical role for coiled coils in the organization of functional protein complexes and corresponding cellular machineries.

Characterization of the coiled-coil network in kinetochore function

The kinetochore is a very important molecular machine responsible for accurate segregation of sister chromosomes during cell division (Kline-Smith *et al.*, 2005; Westermann *et al.*, 2007). In the budding yeast, more than 70 proteins have been identified in the kinetochore that form 14 or more discrete subcomplexes. They are further organized into four categories or layers according to their functions and relative positions in the DNA–microtubule bridge, namely, DNA-binding, linker, microtubule association, and regulatory proteins (McAinsh *et al.*, 2003; Westermann *et al.*, 2007). Despite extensive studies on the kinetochore, its detailed architecture is largely unknown. Our analysis predicted that ~43% of kinetochore proteins contain coiled coils and identified an extensive, coiled-coil–mediated network in the kinetochore that involved 49 coiled-coil–mediated protein interactions (Figure 5). To find out whether these physical interactions are indeed mediated by coiled coils, we first tested by Y2H whether the interactions occur between a coiled-coil motif and its putative protein partner. Out of 76 detected pairs between a

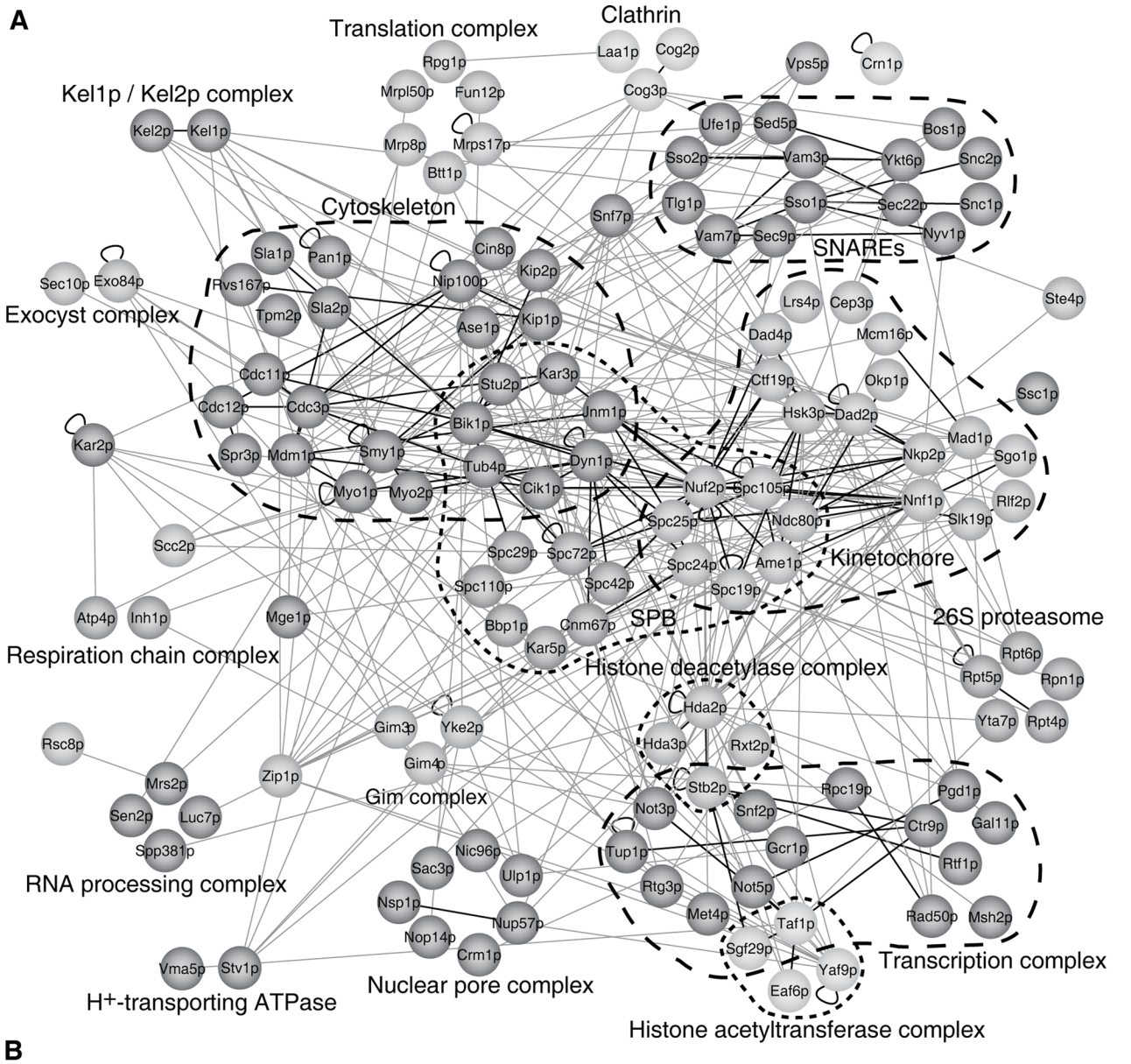

Complex Name	No. proteins	No. coiled-coil proteins	P-value	No. CCMPI	P-value
Cytoskeleton	77	40	<1e-5	28	<0.05
Kinetochore protein complexes	77	33	<1e-5	49	<0.05
Intracellular transport complexes	103	31	<1e-5	23	<1e-5
Genome	6720	637		1777	

FIGURE 4: Organization of coiled-coil–mediated protein interactions into cellular machineries. (A) Coiled-coil–mediated protein interactions are mapped to known yeast protein complexes. The dark black lines indicate CCIs within known protein complexes; the gray lines indicate CCIs between protein complexes; the dashed lines encircle the proteins belonging to the same complex. (B) Three macromolecular complexes, namely, the cytoskeleton, kinetochore, and intracellular protein transport complexes, are significantly enriched in CCPs and their interactions.

coiled coil of one CCP and another CCP (Table S9), 46 pairs were confirmed as positive (60.53%). We then examined the interactions between the corresponding full-length proteins. Using the Y2H and BiFC assay, out of 49 inferred coiled-coil–mediated protein interactions, we tested 44 interactions between their full-length proteins, and 25 coiled-coil–mediated interactions were recapitulated between their parent proteins (~57%). Moreover, a comprehensive literature survey found evidence that supports 11 more interactions at the protein level for the 49 coiled-coil–mediated protein interactions. The recapitulation of a high portion of the 49 coiled-coil–mediated protein interactions we identified in the kinetochore suggests the critical role of coiled coils in the assembly of the molecular machinery. These results are summarized in Table S9. By placing the identified coiled-coil–mediated protein interactions in the context

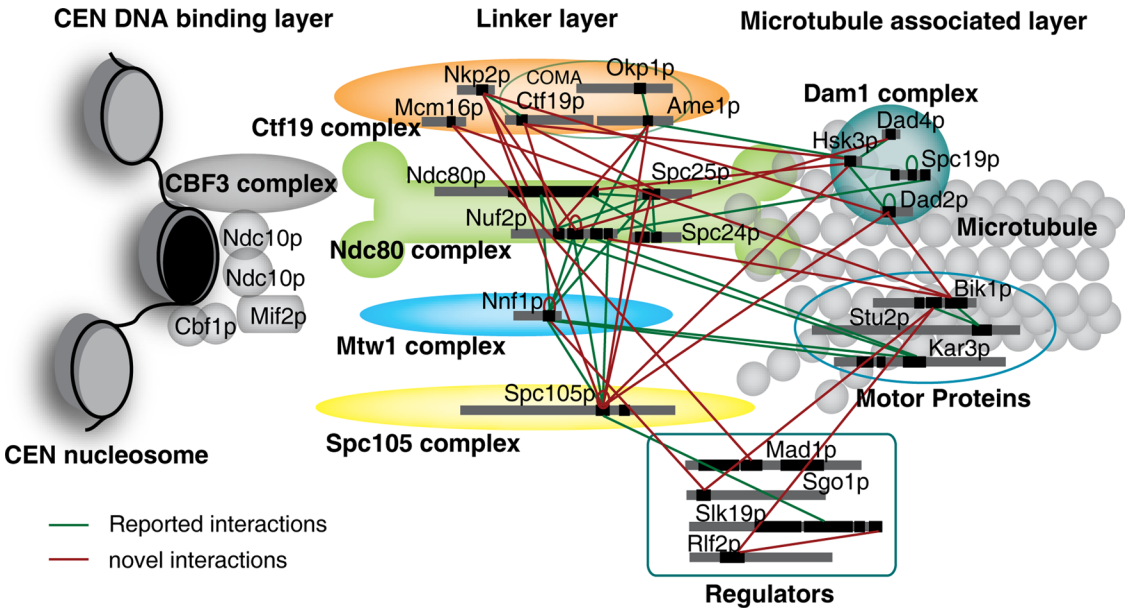

FIGURE 5: A CCI network in the yeast kinetochore. Coiled-coil–mediated interactions in the kinetochore. Each CCP is represented as a gray bar, and its coiled-coil region(s) are indicated using black bar(s). The components within the same subcomplex or category are put in adjacent positions and bordered with simple geometric forms. Lines show interactions between coiled coils. Green lines, previous reported interactions; red lines, novel interactions.

of kinetochore molecular architecture, we found that our network greatly enriched both the intra- and intersubcomplexes association, suggesting that the kinetochore is a highly interwoven structure in which coiled coils play a central role. Of note, in the linker and microtubule association layers, all known major subcomplexes, such as the Ndc80 complex, the Ctf19 complex, and the Dam1 complex, contain at least one CCP that form an interaction network mediated by coiled coils (Figure 5). The most prominent example is found in the Ndc80 complex, in which the four interacting proteins all contain coiled coils that nucleate the complex. This observation is consistent with results from an electron microscopy analysis demonstrating that the long coiled-coil regions of these subunits form a 560-Å-long rod with globular domains on both ends (Wang *et al.*, 2008). We show explicitly that this structure is mediated by CCIs between components of the Ndc80 complex. Moreover, a mesh of CCIs, most of which are novel, were identified between components from different subcomplexes or layers, forming a coiled-coil–based assembly within the kinetochore. The establishment of direct physical associations among linker subcomplexes can be supported by several lines of evidence, such as the cooperation of linker subcomplexes in binding to microtubules (Cheeseman *et al.*, 2006) and the copurification of linker complexes in yeast (Westermann *et al.*, 2003), *Caenorhabditis elegans* (Cheeseman *et al.*, 2004), and humans (Obuse *et al.*, 2004). In addition, coiled coils may also be involved in directing chromosome movement along microtubules, since several coiled-coil associations were observed between the motor proteins and the linker layer proteins and between the components of the linker layer and the Dam1 complexes, suggesting a direct involvement of coiled-coil–mediated interactions in the anchoring and transport of the kinetochore.

Developing network probes for the CCI network

The identification of the CCI network has raised important questions: How is the specificity of the CCIs encoded at a genome level? Can the interaction specificity of the CCI network be explored for functional modifications of the cell? Because of the diverse functions of the CCI network, it is impossible to test these ideas at the CCI interactome level. Given that the CCI and corresponding protein–protein interaction networks in the kinetochore have been well characterized (see Figure 5), we focused on this molecular machinery to explore the functions of the CCI network and to test whether the CCI network could be manipulated to affect cellular behavior, in particular kinetochore assembly and cell growth. The ability to manipulate CCI network in coiled-coil–containing molecular machines may have broad medical relevance, as dysfunction of these molecular machines, as exemplified by the kinetochore, can result in defective cell division and growth (McAinsh *et al.*, 2003). To find out whether disturbance of the coiled coil associations of the kinetochore in budding yeast could lead to cell growth defects, we overexpressed, one at a time, all 30 coiled coils identified to be involved in the kinetochore machinery under the control of the inducible promoter GAL1. We found that the overexpression of two kinetochore coiled coils, namely Ndc80p-cc1 from Ndc80p and Nuf2p-cc2 from Nuf2p, caused significant defects in colony formation (Figure 6A) and retarded cell growth in lipid medium (Figure S7) at 30°C.

We next focused on Ndc80p-cc1 and asked whether the overexpression of a coiled coil indeed affected kinetochore function. By testing the mitotic instability in the cell carrying centromere-containing plasmids, we found that overexpression of Ndc80p-cc1 doubled the rate of the centromere-containing plasmid loss after four generations of growth, with a loss rate reaching as high as 43% (Figure 6B), indicating impairment in chromosome segregation. Flow cytometry analysis showed that the overexpression of Ndc80p-cc1 led to a blockage of cell division at the G2/M phase (Figure 6C). To examine whether the coiled-coil region of Ndc80p is responsible for the interaction between Ndc80p and other kinetochore components, we performed a colocalization analysis between Ndc80p, with or without its coiled-coil region, and Nuf2p. When enhanced green fluorescent protein (EGFP)-Nuf2p was coexpressed with red fluorescent protein (RFP)-tagged Ndc80p (full-length), its coiled-coil

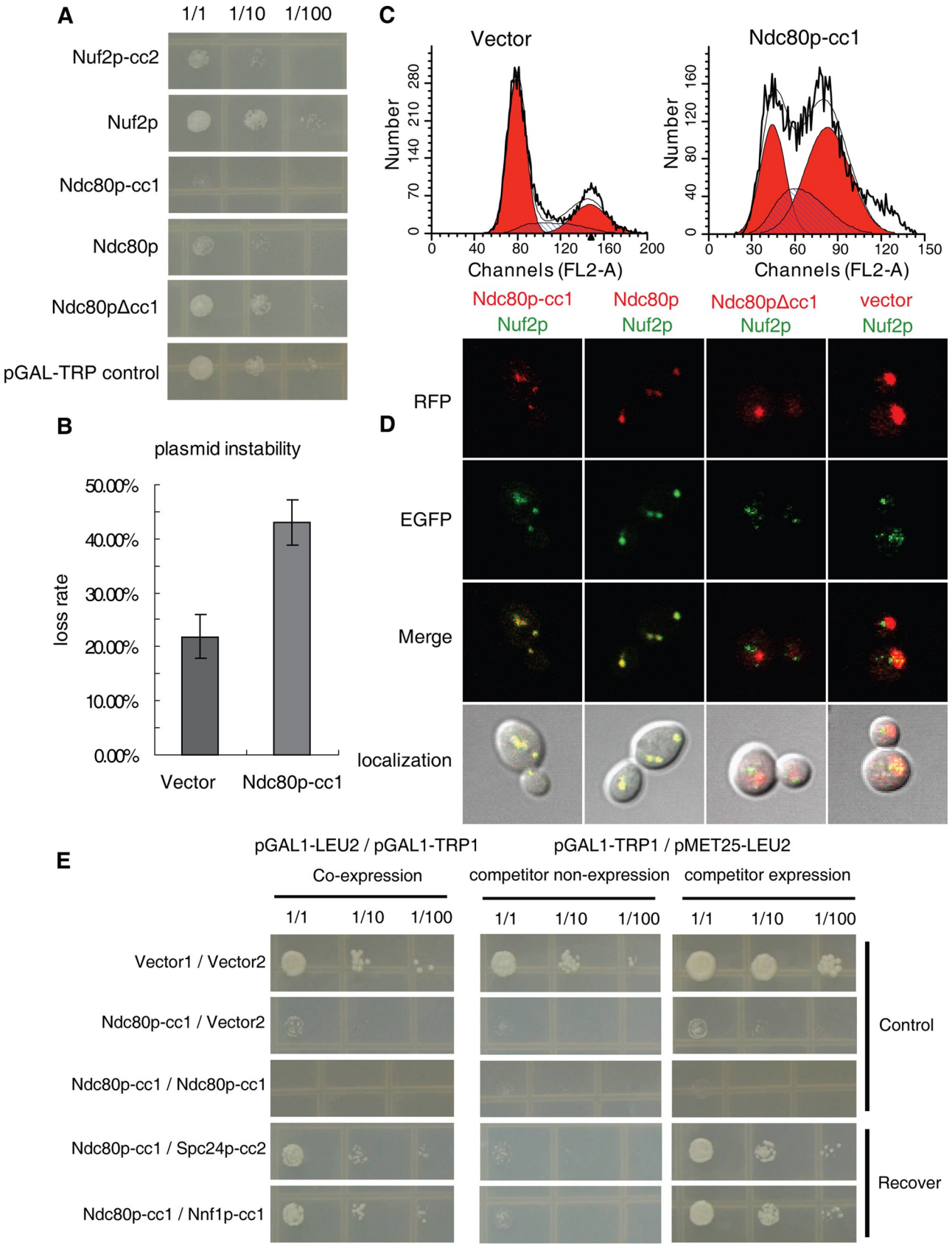

FIGURE 6: Using coiled coils as network probes to modulate the kinetochore CCI network. (A) Cell growth analysis upon overexpression of coiled coils, full-length CCP, and coiled-coil–mutated protein. Nuf2p-cc2 from Nuf2p and Ndc80p-cc1 from Ndc80p caused significant defects in colony formation when overexpressed. The overexpression of the full-length Nuf2p protein did not affect the host cell growth. In contrast, the overexpression of the full-length

region alone (Ndc80p-cc1), or the protein without the coiled-coil region (Ndc80p-Δ-cc1), we found that both the coiled-coil region and the full-length protein colocalized with Nuf2p. In contrast, Ndc80p lacking the coiled-coil region was seen dispersed throughout the nucleus and failed to colocalize with Nuf2 (Figure 6D). These results highlight the importance of the coiled coil of Ndc80p in its proper subcellular localization.

The characterization of coiled-coil–mediated interactions in the kinetochore enabled us to identify specific coiled coils that could function as inhibitors of coiled-coil associations and thereby disrupt kinetochore function. To this end, we investigated whether kinetochore dysfunction caused by a coiled-coil inhibitor could be rescued by reintroduction of its binding partners. A binding partner that rescued the kinetochore function was deemed a *competitor coiled coil* (Figure S8A). For identification of the competitor coiled coils for the inhibitor coiled-coil Ndc80p-cc1, the six interacting partners of Ndc80p in the kinetochore were coexpressed one at a time with Ndc80p-cc1 via a GAL1 promoter. As shown in Figures 6E and S8B, overexpression of Ndc80p-cc1 suppressed cell growth in the absence of competitors (second panel from the top) in a dosage-dependent manner (third panel from the top). Of the six interacting partners, Spc24p-cc2 and Nnf1p-cc1 were identified as competitor coiled coils for Ndc80p-cc1, as they effectively blocked the inhibitory effect of the latter. Furthermore, we developed an in vivo, coiled-coil–based switch to control cell division, which made use of the inducible promoter MET25 to turn on or off expression of a competitor coiled coil. In the absence of the competitor coiled coil, cell growth was efficiently blocked by the inhibitor coiled coil (Figure 6E, second column). In contrast, when the expression of a competitor coiled coil was turned on, cell growth was recovered (Figure 6E, third column). Therefore we argue that it is possible to design network probes, inhibitors, and/or competitors to investigate the function of the CCI network in normal or pathogenic conditions or as candidate therapeutic agents for diseases in which the CCI network is disturbed. Moreover, the CCIs we identified herein may serve as potential molecular circuits to modulate cell growth.

DISCUSSION

Mapping the interactome at the systems level is an important step toward understanding the physiology of an organism. Despite numerous efforts (Uetz *et al.*, 2000; Ito *et al.*, 2001; Gavin *et al.*, 2006; Krogan *et al.*, 2006; Tarassov *et al.*, 2008; Yu *et al.*, 2008), even our understanding of the interactome of budding yeast, the most-studied, single-celled organism, is still far from being complete, due to technical limitations and the complexity of molecular interactions (Hart *et al.*, 2006). The genome-wide analysis of interactions at the motif level offers several advantages that can complement and even outperform, in certain cases, current efforts in large-scale mapping of protein–protein interactions. For example, detection of interactions at the motif level could be more sensitive, thus resulting in a more complete interactome map (Boxem *et al.*, 2008). A whole-genome map of CCIs can also provide unique insights into the binding specificity, biological function, and intracellular distribution of the domain. Previously, researchers have investigated the large-scale interactions for the WW domain, PDZ domain, and other functional domains (Hesselberth *et al.*, 2006; Stiffler *et al.*, 2007). These domains carry out more specialized biological functions and thus tend to have more specific interactions. As we have shown above, although the coiled-coil motif is a general type of interacting domain, its interactions demonstrate a high specificity and tend to mediate functionally related protein interactions. Moreover, as discussed below, detection of interactions at the motif level can provide precise interaction information, enabling a deeper understanding of the mechanism of molecular assembly for certain biological functions.

Systematic analysis of the CCI network has extended our understanding of its roles in the organization and functionality of the cell machinery. We discovered that the coiled-coil motif mediates extensive networking within and between protein complexes in diverse cellular contexts, providing a platform for the organization of cell machinery. Furthermore, we characterized an extensive coiled-coil network within the kinetochore, the components of which are evolutionarily conserved and misconnection of which may cause cancer (Diaz-Rodriguez *et al.*, 2008; Bieche *et al.*, 2011). The coiled-coil network apparently forms a bridge that links the plus end of the microtubule to the centromere DNA. Owing to the dynamic and reversible nature of CCIs, this coiled-coil bridge may assume two roles in kinetochore assembly. It serves as a docking platform that allows dynamic assembly and disassembly of kinetochore components and recruitment of regulatory proteins, such as checkpoint proteins, to the kinetochore (Burke and Stukenberg, 2008). Moreover, it functions as a transmitter that passes force generated by the microtubules to the inner kinetochore, directing the movement of the chromosome to the spindle pole during cell division (Ciferri *et al.*, 2007; Kim *et al.*, 2008). Because many yeast CCPs are conserved in the human proteome, we argue that characterization of the coiled-coil–mediated interactions in budding yeast could provide insights into the functionality of coiled-coil networking in human physiology (Table S10).

The genome-wide study of CCIs also has the potential to be applied in the development of domain-based regulators for network perturbation and pharmacological applications. We utilized the interaction surface in the kinetochore CCI network as a target to

Ndc80p protein caused a significant, but much slighter, effect on cell growth rate compared with Ndc80p-cc1. When the coiled-coil region of Ndc80p was deleted, the construct (Ndc80p-Δ-cc), remarkably, rescued the lethal phenotype. Each coiled coil was named according to its parental protein and its numbering in Table S1. (B) Plasmid instability assay after expression of Ndc80-cc1. A quantitative analysis of plasmid instability shows that overexpression of Ndc80-cc1 doubles the loss rate of the report plasmid, pRS316. (C) Repression of mitotic cell cycle in G2/M phase by Ndc80-cc1 as measured by flow cytometry analysis. Flow cytometry analysis of DNA content in strains carrying either empty vector or Ndc80-cc1 overexpression vector shows a phenotype of G2/M delay upon Ndc80-cc1 overexpression. (D) Fluorescence microscopy analysis of host strains that express the RFP-tagged constructions of Ndc80p-cc1, Ndc80p, or Ndc80p-Δ-cc1 together with the Nuf2p-EGFP. Microscopic analysis shows that Ndc80p-cc1-RFP and Ndc80p-RFP are colocalized with Nuf2p-EGFP, respectively, but that Ndc80p-Δ-cc1-RFP is not colocalized with Nuf2p-EGFP. (E) Design of molecular circuits consisting of Ndc80-cc1 and its interacting partners to regulate cell division. Two competitive expression systems were prepared in this assay. In the first system (first column), the expression of Ndc80-cc1 and its competitor coiled coils were both controlled by the GAL1 promoter. But in the second system (second and third columns), an inducible MET25 promoter was used to turn on and off the expression of competitor coiled coils.

identify potential synthetic coiled-coil–based inhibitors that disturb the structural organization of the kinetochore and found that some coiled coils can indeed repress the activity of the budding yeast kinetochore. Moreover, a coiled-coil–based switch was developed by introducing a competitor coiled coil to bind to the inhibitor coiled coil and rescue the cell from repressed status. These lines of study demonstrate that the domain-level interaction pairs in the coiled-coil network can be used as a general structural scaffold for synthetic pathway design or interaction remodeling.

In conclusion, our work uncovered the largest known coiled-coil interactome for yeast and developed computational strategies to effectively interpret motif-level interaction data. Given the involvement of CCIs in many biological processes and disease pathways, such as viral infection and cancer development (Carr and Kim, 1993; Cully *et al.*, 2005; Eschli *et al.*, 2006), a systematic understanding of coiled coils will facilitate the design of new and effective modulators and therapeutics by targeting the specific, CCIs involved in the targeted process and human disease pathways. Our CCI network data provide a valuable starting-point from which to begin addressing many more questions. For example, how do coiled-coil sequences encode interaction specificity, given the potential of promiscuous binding and the vast network they form? We expect that coiled-coil–targeted interaction screening, together with our domain-based modulator design strategy, may serve as a general platform that is applicable in principle to other motifs and domains. We anticipate that the mapping of the motif/domain-mediated protein–protein interactome will be an essential component of the human proteome project and that such interactome data will eventually lead to the development of interesting applications in pharmacology and synthetic biology.

MATERIALS AND METHODS

Identification and functional analysis of coiled coils in the yeast proteome

Coiled coils were predicted from the yeast genome obtained from the MIPS Comprehensive Yeast Genome Database by using the computer program Paircoil2 with a score cutoff of 0.99 and a window of 28 residues (McDonnell *et al.*, 2006). The functional distribution of the predicted CCPs was analyzed according to GO functional categories (Ashburner *et al.*, 2000) using the Cytoscape plug-in BiNGO 2.4 (Maere *et al.*, 2005). The significance of enrichment of CCPs in each functional category was calculated using the hypergeometric test and Benjamini and Hochberg's false discovery rate correction (Benjamini *et al.*, 2001).

Large-scale screening of CCIs using Y2H

The predicted coiled coils were amplified using PCR from yeast genomic DNA and inserted into the yeast two-hybrid vectors pGBKT7 (bait) and pGADT7-rec (prey) (Clontech, Mountain View, CA). The sequences of each coiled coil were confirmed by DNA sequencing. The screening of CCIs was done in a matrix-mating manner. Each bait strain was mated with all individual prey strains spotted on plates. After 2 d of mating on YPDA (yeast peptone dextrose adenine) media, the colonies were replicated onto selective media SD/-Leu/-Trp plates for selection of diploid cells; these diploid cells were then transferred onto another selective media, SD/-Leu/-Trp/-His/-Ade, for detection of interactions. Colonies were grown at 30°C for 7 d before recording positive results. For elimination of autoactivators, all bait and prey strains were mated with strains of the opposite mating type that contained empty vectors. Two rounds of screening were performed to identify high-confidence interactions. For a more detailed description of the procedure, see the Supplemental Materials.

BiFC assay

The BiFC experiments were done as previously described (Zhang *et al.*, 2009). Briefly, yeast cells containing both N-terminal- and C-terminal fluorescent protein–tagged constructs were cultured in SCR/-Leu/-Trp media (synthetic complete with 2% raffinose) for 40 h at 30°C and then transferred to SCGR/-Leu/-Trp media (synthetic complete with 4% galactose and 2% raffinose) for 24 h at 25°C. After induction, the fluorescence intensities (excitation wavelength Ex = 485 nm, emission wavelength Em = 535 nm) were measured by a microplate reader (GENios Plus; Tecan, Crailsheim, Germany). The experiments were repeated three times under the same conditions, and a pair was scored as positive when the fluorescence intensity of the testing group was significantly higher (p value < 0.05) than the two controls in which one construct was the empty vector.

Computational analysis of the CCI network

Computational analysis of the CCI network topological properties and modularity was carried out by comparing the CCI network with its randomized networks and with the reported coiled-coil protein interaction (CCPI) network. The CCPI network was constructed based on reported physical interactions in the yeast proteome. Data were obtained from DIP (http://dip.doe-mbi.ucla.edu/dip/Download.cgi?SM=7, version Scere 20101010), MIPS (ftp://ftpmips.gsf.de/yeast/PPI, version 18052006), and BioGRID (http://downloads.yeastgenome.org/literature_curation/interaction_data.tab, version 3.1.72) databases. The randomized CCI network was generated by a local rewiring algorithm. Topological analysis of the above networks was carried out by NetworkAnalyzer (Shannon *et al.*, 2003). The functional distribution of coiled-coil–mediated protein interactions and network modularity was analyzed based on GO slim terms. The compilation of yeast protein complexes used in the identification of coiled-coil molecular machines was integrated from the MIPS and SGD databases. For details, see the Supplemental Materials.

Inferring coiled-coil–mediated protein interactions

The 3210 pairs of CCI-derived protein interactions were separated into the following two parts: 1) 196 pairs that overlapped between CCI network and CCPI network were used as positive data; and 2) the remaining 3014 pairs were regarded as unlabeled data. A three-step computational strategy was used to identify coiled-coil–mediated protein interactions from the unlabeled data set. First, we identified several factors (e.g., mRNA expression, protein expression, gene essentiality, and interologues, which transfer conserved protein interaction information across species) that could increase the confidence in inferring coiled-coil–mediated protein interactions. Moreover, several unique factors directly relative to the interactions at the coiled-coil level were also considered in this step (Table S6 and Figure S9), including the coexisting domains with coiled coil, coiled-coil relative length, and CCI specificity as measured by the connectivity of each coiled coil in the CCI network. Second, each pair of CCI-derived proteins was categorized into a bin and represented as a corresponding code for each type of factor. The extent to which each code impacts the odds of whether a protein interacts or not was weighted based on its ability to discriminate between positive data and unlabeled data. This discrimination ability is calculated as a likelihood ratio (L):

$$[L = P(\text{data set}|\text{pos}) \div P(\text{data set}|\text{unlabel})]$$

P(data set|pos) is the probability of observing the code in the positive data set, and P(data set|unlabel) is the probability of observing the code in the unlabeled data set. Finally, a probabilistic model similar to a naïve Bayes was utilized to infer coiled-coil–mediated

protein interactions from CCIs. A confidence score was assigned to each pair of CCI-derived proteins as a joint likelihood ratio. Assuming that the above factors are conditionally independent, we calculated the joint likelihood ratio as the product of those individual likelihood ratios to recognize the high-confidence, coiled-coil–mediated protein interactions:

$$L_{\text{product}}(\text{ConfidenceScore}) = L_1 \times L_2 \times_{\ldots} L_n = P(f_{1\ldots}f_n \mid \text{pos}) \div P(f_{1\ldots}f_n \mid \text{unlabel})$$

For details, see the Supplemental Materials.

Cell growth assay

The yeast strain ySC7 *(MATa, ade2-1 ura3-1 his3-11, 15 trp1-1 leu2-3, 112 can1-100 lys2::hisG bar1::hisG pep4::kanMX)* was used in this assay. Yeast cells transformed with the coiled-coil expression construct pGAL1-TRP1-coild-coil were grown overnight at 30°C in synthetic medium (SC) with 2% glucose; serial dilutions were then made, and the cells were spotted on SC-agar plate with 2% galactose and 1% raffinose. After a 3-d cultivation at 30°C, the colony size was recorded.

To evaluate the growth defect recovery efficiency of the competitor coiled coils, we cotransformed the constructs of Ndc80p-cc1 and its candidate coiled-coil competitors into ySC7. For the pGAL1-LEU2-Ndc80p-cc1/pGAL1-TRP1-competitor-cc pair, the transformants were cultured in SC with 2% glucose overnight and spotted onto the SC with 2% galactose and 1% raffinose. For the pGAL1-TRP1-Ndc80p-cc1/pMET25-LEU2-competitor-cc pair, the cells grown overnight in SC (with 2% glucose) were harvested and spotted onto the inducing SC medium (2% galactose and 1% raffinose) with or without methionine. After a 3-d cultivation at 30°C, the colony size was recorded.

Plasmid instability assay

The yeast ySC7 cells harboring the Ndc80p-cc1 expression construct and a centromere-containing plasmid pRS316 were grown in SC/-TRP-URA medium with 2% glucose at 30°C to mid–log phase (OD600~1). Cells were diluted 1:16 in inducible medium with 2% galactose and 1% raffinose lacking tryptophan, grown for four generations at 30°C, and then plated onto the SC/-URA plate and the YPDA plate, respectively. After a 3-d cultivation at 30°C, colonies were counted, and the loss rate was calculated as the number of cells on the SC/-URA plate divided by the number of cells on the YPDA plate. The test was repeated three times.

Flow cytometry assay

Fluorescence-activated cell sorting was performed as previously described (Zhang and Siede, 2004). Briefly, strains were grown at 30°C to mid–log phase in SC with 2% glucose and then washed and transferred to the inducing medium with 2% galactose and 1% raffinose at the initial concentration of OD_{600} = 0.8. After a 5-h cultivation, ~5×10^6 cells were harvested and fixed in 70% ethanol and stained with propidium iodine at the final concentration of 8 µg/ml. Flow cytometry was then carried out on the FACSCalibur Flow Cytometer (Becton Dickinson Immunocytometry Systems, San Jose, CA).

Fluorescence microscopy

The RFP-tagged constructs of Ndc80p-cc1, Ndc80p, and Ndc80p-Δ-cc1 were cotransformed with plasmid pGAL-LEU2-Nuf2p into ySC7. For microscopic analysis, cells were cultured under the conditions described in *Flow cytometry analysis*. After a 5-h induction, strains were fixed in 4% paraformaldehyde for 15 min, washed twice in 0.1 M KPO_4/1.2 M sorbitol, and then resuspended in *p*-phenylenediamine mounting buffer. The images were captured using a LSCMFV1000 laser-scanning confocal microscope (Olympus, Tokyo, Japan).

ACKNOWLEDGMENTS

We are very grateful to Amy E. Keating for the instruction, discussion, and editing of this work. We thank Joy Fleming for editing the manuscript and members of the Jiang lab for comments on the manuscript. This work was supported by Project "973" (Grant No: 2009CB918503) and the National Foundation of Talent Youth (31125016) to T.J. The funding agencies for this study had no role in study design, data collection and analysis, decision to publish, or preparation of the manuscript.

REFERENCES

Ashburner M, *et al.* (2000). Gene Ontology: tool for the unification of biology. The Gene Ontology Consortium. Nat Genet 25, 25–29.

Barabasi AL, Oltvai ZN (2004). Network biology: understanding the cell's functional organization. Nat Rev Genet 5, 101–113.

Benjamini Y, Drai D, Elmer G, Kafkafi N, Golani I (2001). Controlling the false discovery rate in behavior genetics research. Behav Brain Res 125, 279–284.

Bertin A, McMurray MA, Grob P, Park SS, Garcia G, III, Patanwala I, Ng HL, Alber T, Thorner J, Nogales E (2008). *Saccharomyces cerevisiae* septins: supramolecular organization of heterooligomers and the mechanism of filament assembly. Proc Natl Acad Sci USA 105, 8274–8279.

Bieche I, *et al.* (2011). Expression analysis of mitotic spindle checkpoint genes in breast carcinoma: role of NDC80/HEC1 in early breast tumorigenicity, and a two-gene signature for aneuploidy. Mol Cancer 10, 23.

Boato F, Thomas RM, Ghasparian A, Freund-Renard A, Moehle K, Robinson JA (2007). Synthetic virus-like particles from self-assembling coiled-coil lipopeptides and their use in antigen display to the immune system. Angew Chem Int Ed Engl 46, 9015–9018.

Boxem M, *et al.* (2008). A protein domain-based interactome network for *C. elegans* early embryogenesis. Cell 134, 534–545.

Bromley EH, Channon K, Moutevelis E, Woolfson DN (2008). Peptide and protein building blocks for synthetic biology: from programming biomolecules to self-organized biomolecular systems. ACS Chem Biol 3, 38–50.

Burke DJ, Stukenberg PT (2008). Linking kinetochore-microtubule binding to the spindle checkpoint. Dev Cell 14, 474–479.

Carr CM, Kim PS (1993). A spring-loaded mechanism for the conformational change of influenza hemagglutinin. Cell 73, 823–832.

Cheeseman IM, Chappie JS, Wilson-Kubalek EM, Desai A (2006). The conserved KMN network constitutes the core microtubule-binding site of the kinetochore. Cell 127, 983–997.

Cheeseman IM, Niessen S, Anderson S, Hyndman F, Yates JR, III, Oegema K, Desai A (2004). A conserved protein network controls assembly of the outer kinetochore and its ability to sustain tension. Genes Dev 18, 2255–2268.

Ciferri C, Musacchio A, Petrovic A (2007). The Ndc80 complex: hub of kinetochore activity. FEBS Lett 581, 2862–2869.

Crick FHC (1953). The packing of alpha-helices—simple coiled-coils. Acta Crystallogr 6, 689–697.

Cully M, Shiu J, Piekorz RP, Muller WJ, Done SJ, Mak TW (2005). Transforming acidic coiled coil 1 promotes transformation and mammary tumorigenesis. Cancer Res 65, 10363–10370.

Diaz-Rodriguez E, Sotillo R, Schvartzman JM, Benezra R (2008). Hec1 overexpression hyperactivates the mitotic checkpoint and induces tumor formation in vivo. Proc Natl Acad Sci USA 105, 16719–16724.

Eschli B, Quirin K, Wepf A, Weber J, Zinkernagel R, Hengartner H (2006). Identification of an N-terminal trimeric coiled-coil core within arenavirus glycoprotein 2 permits assignment to class I viral fusion proteins. J Virol 80, 5897–5907.

Gavin AC, *et al.* (2006). Proteome survey reveals modularity of the yeast cell machinery. Nature 440, 631–636.

Gillingham AK, Munro S (2003). Long coiled-coil proteins and membrane traffic. Biochim Biophys Acta 1641, 71–85.

Grigoryan G, Reinke AW, Keating AE (2009). Design of protein-interaction specificity gives selective bZIP-binding peptides. Nature 458, 859–864.

Hart GT, Ramani AK, Marcotte EM (2006). How complete are current yeast and human protein-interaction networks? Genome Biol 7, 120.
Hesselberth JR, Miller JP, Golob A, Stajich JE, Michaud GA, Fields S (2006). Comparative analysis of *Saccharomyces cerevisiae* WW domains and their interacting proteins. Genome Biol 7, R30.
Hu CD, Chinenov Y, Kerppola TK (2002). Visualization of interactions among bZIP and Rel family proteins in living cells using bimolecular fluorescence complementation. Mol Cell 9, 789–798.
Ito T, Chiba T, Ozawa R, Yoshida M, Hattori M, Sakaki Y (2001). A comprehensive two-hybrid analysis to explore the yeast protein interactome. Proc Natl Acad Sci USA 98, 4569–4574.
Jahn R, Scheller RH (2006). SNAREs—engines for membrane fusion. Nat Rev Mol Cell Biol 7, 631–643.
Kerppola TK (2008). Bimolecular fluorescence complementation (BiFC) analysis as a probe of protein interactions in living cells. Annu Rev Biophys 37, 465–487.
Kilby JM, *et al*. (1998). Potent suppression of HIV-1 replication in humans by T-20, a peptide inhibitor of gp41-mediated virus entry. Nat Med 4, 1302–1307.
Kim Y, Heuser JE, Waterman CM, Cleveland DW (2008). CENP-E combines a slow, processive motor and a flexible coiled coil to produce an essential motile kinetochore tether. J Cell Biol 181, 411–419.
Kline-Smith SL, Sandall S, Desai A (2005). Kinetochore-spindle microtubule interactions during mitosis. Curr Opin Cell Biol 17, 35–46.
Komurov K, White M (2007). Revealing static and dynamic modular architecture of the eukaryotic protein interaction network. Mol Syst Biol 3, 110.
Krogan NJ, *et al*. (2006). Global landscape of protein complexes in the yeast *Saccharomyces cerevisiae*. Nature 440, 637–643.
Liu J, Rost B (2001). Comparing function and structure between entire proteomes. Protein Sci 10, 1970–1979.
Lomander A, Hwang W, Zhang S (2005). Hierarchical self-assembly of a coiled-coil peptide into fractal structure. Nano Lett 5, 1255–1260.
Lupas A, Van Dyke M, Stock J (1991). Predicting coiled coils from protein sequences. Science 252, 1162–1164.
Lupas AN, Gruber M (2005). The structure of α-helical coiled coils. Adv Protein Chem 70, 37–78.
Maere S, Heymans K, Kuiper M (2005). BiNGO: a Cytoscape plugin to assess overrepresentation of Gene Ontology categories in biological networks. Bioinformatics 21, 3448–3449.
Mason JM, Schmitz MA, Muller KM, Arndt KM (2006). Semirational design of Jun-Fos coiled coils with increased affinity: universal implications for leucine zipper prediction and design. Proc Natl Acad Sci USA 103, 8989–8994.
McAinsh AD, Tytell JD, Sorger PK (2003). Structure, function, and regulation of budding yeast kinetochores. Annu Rev Cell Dev Biol 19, 519–539.
McDonnell AV, Jiang T, Keating AE, Berger B (2006). Paircoil2: improved prediction of coiled coils from sequence. Bioinformatics 22, 356–358.
McFarlane AA, Orriss GL, Stetefeld J (2009). The use of coiled-coil proteins in drug delivery systems. Eur J Pharmacol 625, 101–107.
Newman JR, Wolf E, Kim PS (2000). A computationally directed screen identifying interacting coiled coils from *Saccharomyces cerevisiae*. Proc Natl Acad Sci USA 97, 13203–13208.
O'Shea EK, Klemm JD, Kim PS, Alber T (1991). X-ray structure of the GCN4 leucine zipper, a two-stranded, parallel coiled coil. Science 254, 539–544.
O'Shea EK, Rutkowski R, Kim PS (1992). Mechanism of specificity in the Fos-Jun oncoprotein heterodimer. Cell 68, 699–708.
Obuse C, Iwasaki O, Kiyomitsu T, Goshima G, Toyoda Y, Yanagida M (2004). A conserved Mis12 centromere complex is linked to heterochromatic HP1 and outer kinetochore protein Zwint-1. Nat Cell Biol 6, 1135–1141.
Parry DA (1982). Coiled-coils in alpha-helix-containing proteins: analysis of the residue types within the heptad repeat and the use of these data in the prediction of coiled-coils in other proteins. Biosci Rep 2, 1017–1024.
Ravasz E, Somera AL, Mongru DA, Oltvai ZN, Barabasi AL (2002). Hierarchical organization of modularity in metabolic networks. Science 297, 1551–1555.
Robson Marsden H, Kros A (2010). Self-assembly of coiled coils in synthetic biology: inspiration and progress. Angew Chem Int Ed Engl 49, 2988–3005.
Rose A, Meier I (2004). Scaffolds, levers, rods and springs: diverse cellular functions of long coiled-coil proteins. Cell Mol Life Sci 61, 1996–2009.
Schliwa M, Woehlke G (2003). Molecular motors. Nature 422, 759–765.
Shannon P, Markiel A, Ozier O, Baliga NS, Wang JT, Ramage D, Amin N, Schwikowski B, Ideker T (2003). Cytoscape: a software environment for integrated models of biomolecular interaction networks. Genome Res 13, 2498–2504.
Shekhawat SS, Porter JR, Sriprasad A, Ghosh I (2009). An autoinhibited coiled-coil design strategy for split-protein protease sensors. J Am Chem Soc 131, 15284–15290.
Shlizerman C, Atanassov A, Berkovich I, Ashkenasy G, Ashkenasy N (2010). De novo designed coiled-coil proteins with variable conformations as components of molecular electronic devices. J Am Chem Soc 132, 5070–5076.
Stiffler MA, Chen JR, Grantcharova VP, Lei Y, Fuchs D, Allen JE, Zaslavskaia LA, MacBeath G (2007). PDZ domain binding selectivity is optimized across the mouse proteome. Science 317, 364–369.
Strauss HM, Keller S (2008). Pharmacological interference with protein-protein interactions mediated by coiled-coil motifs. In: Protein-Protein Interactions as New Drug Targets, ed. E Klussmann and J Scott, Handbook of Experimental Pharmacology, Vol. 186, Berlin: Springer, 461–482.
Tarassov K, Messier V, Landry CR, Radinovic S, Serna Molina MM, Shames I, Malitskaya Y, Vogel J, Bussey H, Michnick SW (2008). An in vivo map of the yeast protein interactome. Science 320, 1465–1470.
Uetz P *et al*. (2000). A comprehensive analysis of protein-protein interactions in *Saccharomyces cerevisiae*. Nature 403, 623–627.
Ungar D, Hughson FM (2003). SNARE protein structure and function. Annu Rev Cell Dev Biol 19, 493–517.
Wang HW, Long S, Ciferri C, Westermann S, Drubin D, Barnes G, Nogales E (2008). Architecture and flexibility of the yeast Ndc80 kinetochore complex. J Mol Biol 383, 894–903.
Westermann S, Cheeseman IM, Anderson S, Yates JR, III, Drubin DG, Barnes G (2003). Architecture of the budding yeast kinetochore reveals a conserved molecular core. J Cell Biol 163, 215–222.
Westermann S, Drubin DG, Barnes G (2007). Structures and functions of yeast kinetochore complexes. Annu Rev Biochem 76, 563–591.
Wild C, Oas T, McDanal C, Bolognesi D, Matthews T (1992). A synthetic peptide inhibitor of human immunodeficiency virus replication: correlation between solution structure and viral inhibition. Proc Natl Acad Sci USA 89, 10537–10541.
Wu K, Liu J, Johnson RN, Yang J, Kopecek J (2009). Drug-free macromolecular therapeutics: induction of apoptosis by coiled-coil-mediated cross-linking of antigens on the cell surface. Angew Chem Int Ed Engl 49, 1451–1455.
Yu H *et al*. (2008). High-quality binary protein interaction map of the yeast interactome network. Science 322, 104–110.
Zhang H, Chen J, Wang Y, Peng L, Dong X, Lu Y, Keating AE, Jiang T (2009). A computationally guided protein-interaction screen uncovers coiled-coil interactions involved in vesicular trafficking. J Mol Biol 392, 228–241.
Zhang H, Siede W (2004). Analysis of the budding yeast *Saccharomyces cerevisiae* cell cycle by morphological criteria and flow cytometry. Methods Mol Biol 241, 77–91.